Research Article Vol. 9, No. 10 / October 2021 / Photonics Research 1939

PHOTONICS Research

Terahertz wavefront shaping with multi-channel polarization conversion based on all-dielectric metasurface

Jie Li,[1] Chenglong Zheng,[1] Jitao Li,[1] Guocui Wang,[2,3] Jingyu Liu,[2] Zhen Yue,[1] Xuanruo Hao,[1] Yue Yang,[1] Fuyu Li,[4] Tingting Tang,[4] Yating Zhang,[1,5] Yan Zhang,[2,6] and Jianquan Yao[1,7]

[1]Key Laboratory of Opto-Electronics Information Technology (Tianjin University), Ministry of Education, School of Precision Instruments and Opto-Electronics Engineering, Tianjin University, Tianjin 300072, China
[2]Beijing Key Laboratory for Metamaterials and Devices, Key Laboratory of Terahertz Optoelectronics, Ministry of Education, and Beijing Advanced Innovation Center for Imaging Technology, Department of Physics, Capital Normal University, Beijing 100048, China
[3]Beijing Engineering Research Center for Mixed Reality and Advanced Display, School of Optics and Photonics, Beijing Institute of Technology, Beijing 100081, China
[4]Information Materials and Device Applications Key Laboratory of Sichuan Provincial Universities, Chengdu University of Information Technology, Chengdu 610225, China
[5]e-mail: yating@tju.edu.cn
[6]e-mail: yzhang@mail.cnu.edu.cn
[7]e-mail: jqyao@tju.edu.cn

Received 10 May 2021; revised 8 July 2021; accepted 24 July 2021; posted 26 July 2021 (Doc. ID 431019); published 13 September 2021

Polarization manipulation of electromagnetic wave or polarization multiplexed beam shaping based on metasurfaces has been reported in various frequency bands. However, it is difficult to shape the beam with multi-channel polarization conversion in a single metasurface. Here, we propose a new method for terahertz wavefront shaping with multi-channel polarization conversion via all-silicon metasurface, which is based on the linear shape birefringence effect in spatially interleaved anisotropic meta-atoms. By superimposing the eigen- and non-eigen-polarization responses of the two kinds of meta-atoms, we demonstrate the possibility for high-efficiency evolution of several typical polarization states with two independent channels for linearly polarized waves. The measured polarization conversion efficiency is higher than 70% in the range of 0.9–1.3 THz, with a peak value of 89.2% at 1.1 THz. In addition, when more other polarization states are incident, combined with the integration of sub-arrays, we can get more channels for both polarization conversion and beam shaping. Simulated and experimental results verify the feasibility of this method. The proposed method provides a new idea for the design of terahertz multi-functional metadevices.

https://doi.org/10.1364/PRJ.431019

1. INTRODUCTION

Polarization is an important variable of electromagnetic waves, typical types of which include linear, circular, and elliptical ones. From the perspective of electromagnetic field, it refers to the trajectory of the electric field vibration, and from the perspective of the photons, it (circular polarization) can also be related to the spin angular momentum [1,2]. Therefore, polarization of light has been widely studied and applied in imaging, quantum optics, and other fields, and polarization manipulation has become an important research content of modern optics and photonics [3–5]. Traditional optical devices based on bulk crystals are used for polarization generation or conversion, such as polarizers and wave plates. The wave plate is based on the linear birefringence effect of the optical crystal, which produces a phase shift between the ordinary and the extraordinary components with an appropriate thickness, and then superimposes them into a new polarization. Such devices are large in size and require high processing accuracy, while only specific materials can be used in each electromagnetic band [6]. More importantly, these devices can hardly realize the simultaneous control of other optical parameters while performing polarization conversion, such as amplitude and phase. This is not conducive to the multi-functional and integrated development of modern optical devices.

Electromagnetic metasurfaces are planar functional devices composed of artificially designed sub-wavelength meta-atoms [7–10]. After more than 10 years of rapid development, significant progress of them has been made in the fields of

information optics [11,12], quantum optics [4,5], non-linear optics, and terahertz photonics [13–17]. Electromagnetic functional devices based on metasurfaces are flexible in design and conducive for integration. They not only provide new ideas for the development of new optical devices, but also provide powerful tools for many basic physics researches [18–20]. In particular, metasurfaces also achieve optical linear birefringence and polarization conversion. Different from the material birefringence of traditional optical devices, the meta-atoms in metasurface utilize the shape birefringence [21], which has been realized from microwave to ultraviolet bands using a dielectric or metal [22,23]. For shape-induced linear birefringence, when the incident polarization is consistent with the symmetry axis of the anisotropic meta-atom, the output polarization state remains unchanged, and the incident polarization state is called the eigen-polarization state. When the other linearly polarized wave is incident, its projection in the eigen-polarization state will cause polarization transformation [21], and the output polarization state can be designed by changing the geometric parameters of the structure. The advantage of shape birefringence is that the working frequency can be designed, and other functions can be achieved with polarization conversion, such as non-linear effect [10], wavefront shaping [5,24,25], and polarization-dependent beam energy distribution [26,27]. In particular, researchers set the appropriate geometric dimensions to make the linear polarization conversion efficiency of the meta-atoms be about 50%, controlled the phase difference between the co- and cross-polarized components, and then obtained beam shaping with designed polarization [28–30]. This method is similar to the principle of a quarter-wave plate and can realize the polarization conversion with a simple structure, but the transformation channels are non-independent due to the symmetry of the meta-atoms. It is difficult to achieve independent polarization conversion between different channels. In addition to the linear polarization-based approach, the circular polarization-based one has also been reported, that is, the phase manipulation method of spin decoupling which combines geometric and dynamic phases, while the cross- and co-polarizations can be controlled at the same time [31–33]. However, the optical response of each unit needs to meet several conditions at the same time, which means that their design process is complicated. Therefore, metadevices for polarization conversion with a simple design and two or more independent channels are very necessary.

Here, we propose a new method for terahertz beam shaping with multiple polarization conversion channels. Two sets of spatially interleaved anisotropic units are used to obtain the linearly co- and cross-polarized components, which are superimposed to obtain a new polarization state in beam shaping. We take the focused beam as an example to improve the signal-to-noise ratio (SNR) of the measurement for terahertz electric field. We use two samples to demonstrate the high-efficiency, broadband polarization conversion and the multi-channel function brought about by the incident polarization and the sub-arrays. This method is not only suitable for design of linear polarization-based metasurfaces, but also can be extended to circular polarization-based devices.

2. RESULTS AND DISCUSSION

The proposed scheme of beam shaping with polarization conversion is shown in Fig. 1, in which Fig. 1(a) is a schematic diagram of the metasurface. We take the incidence of two orthogonal linear polarization states as an example (such as x and y polarizations). In the transmitted wave, we can obtain two independent polarization states, such as different linear or circular polarizations. Here we define the polarization states with an angle of 45° or −45° to the x axis as "a" or "b" polarization, respectively [28]. The above-mentioned functions are realized by the spatially interleaved structure shown in Fig. 1(b), in which the two kinds of units differ by half a period ($p/2$) in both the x and y directions. When an x- or y-polarized wave is incident, the transmitted wave of the cross-ellipse cylinder [structure (i)] maintains its polarization state, which is called the eigen-polarization. Moreover, the transmission phases of the two polarization states can be independently controlled. For structure (ii), the long axis of the ellipse forms an angle of 45° or −45° with respect to the x axis, and its eigen-polarization states are a and b polarizations. The transmitted wave can be efficiently converted into cross-polarization when x- or y-polarized beam is incident. In this way, we have three polarization components to control, and then two independent polarization channels can be obtained after superposition. In addition, other incident polarization states can be regarded as vector superposition of x and y polarizations with a specific phase shift, so more transmission polarization states can also be obtained. For example, when a/b-polarized waves are incident, the transmitted waves will be elliptically polarized.

Here, we make a brief theoretical analysis of the working principle for the metasurface in Fig. 1. Without loss of generality, we consider the condition of x or y polarization incidence. Considering that there are two kinds of units in our metasurface, the operational relationship between the transmitted and incident electric field is

$$\begin{pmatrix} E_t^x \\ E_t^y \end{pmatrix} = \begin{pmatrix} T_{xx} & T_{xy} \\ T_{yx} & T_{yy} \end{pmatrix} \begin{pmatrix} E_i^x \\ E_i^y \end{pmatrix}, \tag{1}$$

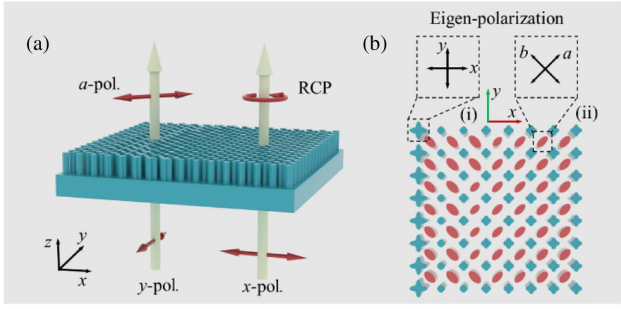

Fig. 1. Schematic diagram of the metasurface for beam shaping with dual-channel polarization conversion. (a) Taking the orthogonal linearly polarized terahertz waves as an example, a 45° polarized (a-polarized) or right circularly polarized (RCP) beam can be obtained when the x- or y-polarized wave is incident, respectively. (b) The arrangement of two types of meta-atoms in the metasurface. The eigen-polarizations for the first and second types of meta-atoms are x (y) polarization and ±45° (a, b) polarizations, respectively.

where the matrix $\boldsymbol{T}$ is the transmission matrix of the meta-atoms, and its elements T_{ij} $(i,j=x,y)$ represent the transmission coefficients. When the polarization conversion efficiency of the second type meta-atoms is high enough, the unconverted part can be ignored, and the matrix $\boldsymbol{T}$ can be decomposed into the sum of the co- and cross-polarization components:

$$\boldsymbol{T}=\boldsymbol{T}_{\mathrm{co}}+\boldsymbol{T}_{\mathrm{cross}}=\begin{pmatrix}T_{xx}&0\\0&T_{yy}\end{pmatrix}+\begin{pmatrix}0&T_{xy}\\T_{yx}&0\end{pmatrix}. \tag{2}$$

The transmission coefficient T_{ij} can be written as the product of its modulus and phase, namely,

$$\begin{aligned}\boldsymbol{T}&=\boldsymbol{T}_{\mathrm{co}}+\boldsymbol{T}_{\mathrm{cross}}\\&=\begin{pmatrix}t_{xx}\varphi_{xx}&0\\0&t_{yy}\varphi_{yy}\end{pmatrix}+\begin{pmatrix}0&t_{xy}\varphi_{xy}\\t_{yx}\varphi_{yx}&0\end{pmatrix}.\end{aligned} \tag{3}$$

In our structure (ii), the angle between the long axis of the ellipse and the x axis is 45° or −45°, so $t_{xy}\cdot\varphi_{xy}=t_{yx}\cdot\varphi_{yx}$; then the two coefficients can be unified as $t_{\mathrm{cross}}\cdot\varphi_{\mathrm{cross}}$.

When the x-polarized wave is incident, we have

$$\begin{aligned}\begin{pmatrix}E_t^x\\E_t^y\end{pmatrix}&=\begin{pmatrix}T_{xx}&T_{xy}\\T_{yx}&T_{yy}\end{pmatrix}\begin{pmatrix}E_i^x\\0\end{pmatrix}=\begin{pmatrix}T_{xx}&E_i^x\\T_{yx}&E_i^x\end{pmatrix}\\&=\begin{pmatrix}t_{xx}\varphi_{xx}&E_i^x\\t_{\mathrm{cross}}\varphi_{\mathrm{cross}}&E_i^x\end{pmatrix}.\end{aligned} \tag{4}$$

Assuming that the phase difference between the transmitted x- and y-polarized components is $\Delta\varphi_x=\varphi_{\mathrm{co}}-\varphi_{\mathrm{cross}}=\varphi_{xx}-\varphi_{\mathrm{cross}}$, and the transmission amplitude is 1, then the total transmitted electric field is

$$\boldsymbol{E}_t^{(1)}=(\varphi_{\mathrm{cross}}+\Delta\varphi_x)E_i^x\cdot\boldsymbol{i}_x+\varphi_{\mathrm{cross}}E_i^x\cdot\boldsymbol{i}_y, \tag{5}$$

where $\boldsymbol{i}_x$ and $\boldsymbol{i}_y$ are unit vectors in the x and y directions.

Similarly, when the y-polarized wave is incident, the transmitted electric field is

$$\begin{aligned}\begin{pmatrix}E_t^x\\E_t^y\end{pmatrix}&=\begin{pmatrix}T_{xx}&T_{xy}\\T_{yx}&T_{yy}\end{pmatrix}\begin{pmatrix}0\\E_i^y\end{pmatrix}=\begin{pmatrix}T_{xy}&E_i^y\\T_{yy}&E_i^y\end{pmatrix}\\&=\begin{pmatrix}t_{\mathrm{cross}}\varphi_{\mathrm{cross}}&E_i^y\\t_{yy}\varphi_{yy}&E_i^y\end{pmatrix}.\end{aligned} \tag{6}$$

The phase difference between the transmitted x- and y-polarized components at this time is $\Delta\varphi_y=\varphi_{\mathrm{co}}-\varphi_{\mathrm{cross}}=\varphi_{yy}-\varphi_{\mathrm{cross}}$, and the transmission amplitude is 1:

$$\boldsymbol{E}_t^{(2)}=\varphi_{\mathrm{cross}}E_i^y\cdot\boldsymbol{i}_x+(\varphi_{\mathrm{cross}}+\Delta\varphi_y)E_i^y\cdot\boldsymbol{i}_y. \tag{7}$$

It can be seen from Eqs. (5) and (7) that when we fix the phase of cross-polarization, the total output electric field is determined by $\Delta\varphi_y$ and $\Delta\varphi_x$, which means that the transmission polarization state is also determined by them.

In order to obtain the above-mentioned metasurface, we use commercial numerical simulation software to obtain parameter libraries of the two kinds of meta-atoms. We choose high-resistance silicon as the constituent material, and process meta-atoms directly on the silicon wafer. High-resistance silicon ($\rho>5000\ \Omega\cdot\mathrm{m}$) shows almost no absorption for terahertz wave, and its dielectric constant is set as $\varepsilon=11.9$ during the simulation. The two structures are shown in Fig. 2(a), where the period is $p=140$ μm, the height of the silicon pillar is $h=200$ μm, and the thickness of the substrate is 300 μm.

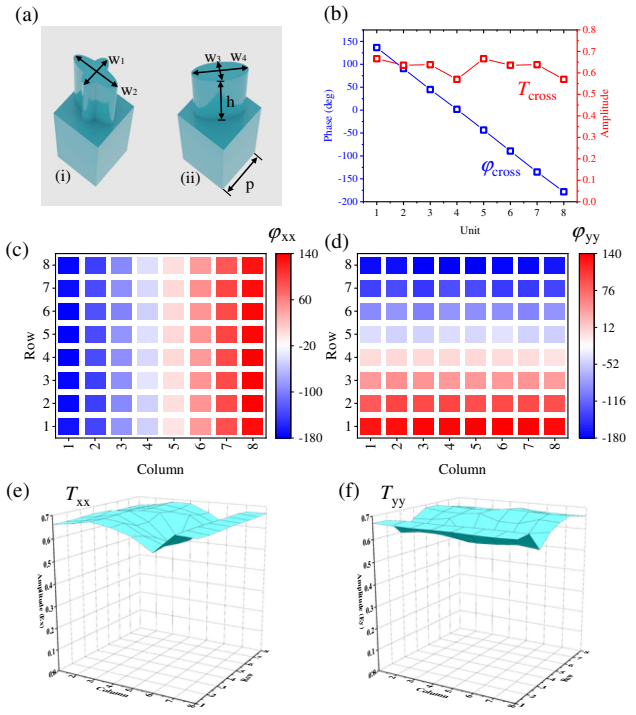

Fig. 2. Amplitudes and phases of the transmitted wave corresponding to meta-atoms with selected geometric parameters. (a) Geometric shape of the two kinds of meta-atoms. Amplitude and phase values for the (b) second and (c)–(f) first types of meta-atoms.

The major and minor axes of the ellipse in structure (ii) are w_4 and w_3, respectively. The minor axes of the two ellipses in structure (i) are both $D=40$ μm, and the major axes are w_1 and w_2, respectively.

By scanning the parameters of the two structures (the original data can be seen in Appendix B, Fig. 6, the working frequency is $f=1.1$ THz), we first obtained the parameter library of structure (ii), as shown in Fig. 2(b). Since the structure will generate y- and x-polarized waves that are equal in value when the x and y polarizations are incident, respectively, we use only one component to represent them uniformly (T_{cross} and φ_{cross}). The phase shifts of the eight elements are changed from 135° to 180°, which is equivalent to covering the interval of [−180°, 180°] with a step of 45°. The first-order transmission coefficients of the eight elements are all around 0.6. The parameter library of structure (i) is shown in Figs. 2(c)–2(f); the values in the figure are obtained by probing the co-polarization components when x- or y-polarized waves are incident separately. Each unit in the library needs to consider the transmission phase shifts for both x- and y-polarized waves (eigen-polarizations) at the same time, and the amplitude remains the same. It can be seen from the figure that the selected phases show a good gradient with a step of 45°, and the first-order amplitudes of all units basically remain above 0.6. The transmission efficiency limitation of the two types of structures is mainly due to the reflection at the air/silicon interface.

Based on the above parameter library, we design two metasurfaces to verify the beam shaping with polarization

conversion. The samples are processed from a 500 μm thick high-resistance silicon through inductively coupled plasma (ICP) etching technology. Each sample is a square with a side length of 1.4 cm. The specific processing steps can be seen in Appendix A. The scanning electron microscope (SEM) images of the first metasurface are shown in Fig. 3(a), which is called sample 1. Its effective area is a circular array composed of the two kinds of meta-atoms mentioned above. There are 80 units (1.12 cm) of each kind in the radial direction. It can be seen from the figure that the sidewalls of the meta-atoms are very steep, which means the processing error is not obvious. In order to illustrate the polarization conversion function of sample 1 intuitively, we use Poincaré spheres to show the incident and transmission polarization states, which are denoted by $|\text{in}\rangle$ and $|\text{out}\rangle$, respectively, as shown in Fig. 3(b). To show the independence of the two polarization channels, we hope that when the x- and y-polarized waves are incident, the transmission waves are a-polarized or right circularly polarized (RCP), respectively. In addition, we design the transmitted beam as a focused vortex beam, which can improve the SNR of the measurement results. Therefore, the expression of the phase profile of the three channels in the metasurface should be

$$\bar{\varphi}_{xx} = -\left(\frac{2\pi}{\lambda}\sqrt{x^2+y^2+f^2}-f\right)+\arctan\left(\frac{y}{x}\right)-\frac{\pi}{2}, \tag{8}$$

$$\bar{\varphi}_{yy} = -\left(\frac{2\pi}{\lambda}\sqrt{x^2+y^2+f^2}-f\right)+\arctan\left(\frac{y}{x}\right), \tag{9}$$

$$\bar{\varphi}_{\text{cross}} = -\left(\frac{2\pi}{\lambda}\sqrt{\left(x+\frac{p}{2}\right)^2+\left(y-\frac{p}{2}\right)^2+f^2}-f\right)+\arctan\left(\frac{y}{x}\right), \tag{10}$$

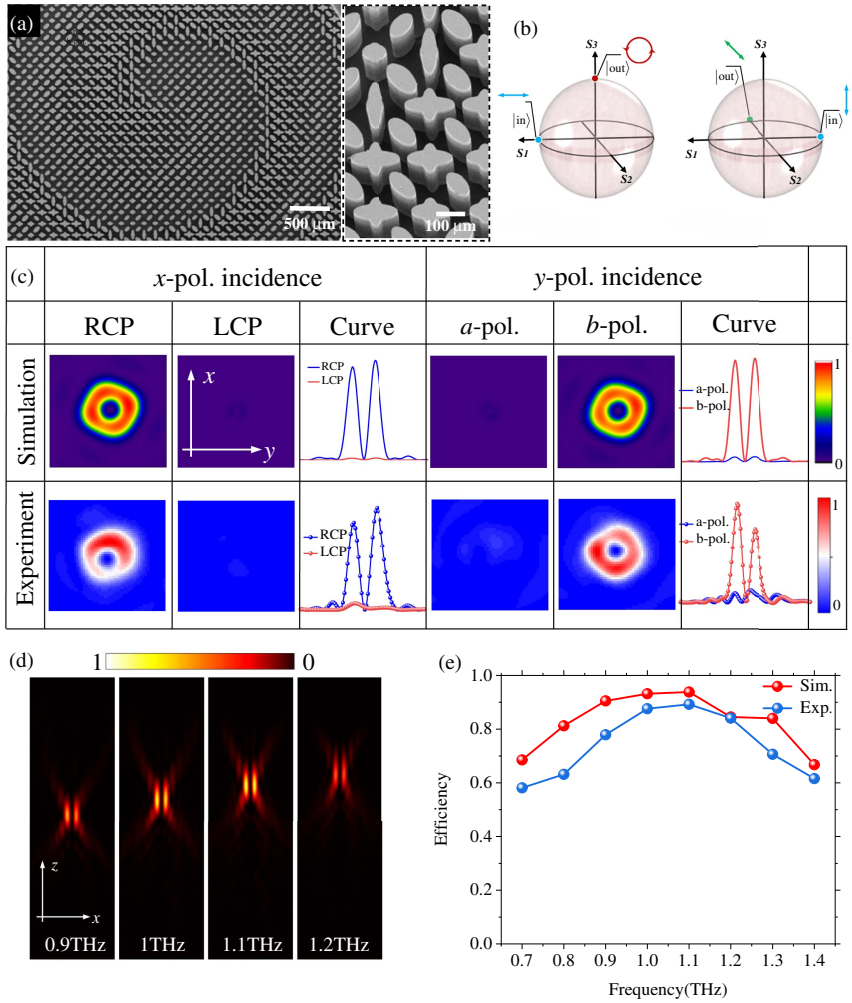

Fig. 3. Simulated and experimental results of sample 1 for the generation of focused vortex beam with polarization conversion. (a) SEM images of sample 1. (b) Demonstration of dual-channel polarization conversion on the Poincaré sphere. (c) Electric field intensity of the transmitted wave in the focal plane when the x- or y-polarized beam is incident. (d) Electric field intensity in the longitudinal section (xoz-plane) at different frequencies. (e) The simulated and measured polarization conversion efficiency of the metasurface in the range of 0.7–1.4 THz at the focal plane, in which the designed working frequency is 1.1 THz.

where $\bar{\varphi}_{xx}$ and $\bar{\varphi}_{yy}$ are responses for the x- or y-polarized wave of structure (i), and $\bar{\varphi}_{\text{cross}}$ is the phase response of structure (ii). In order to eliminate the influence of spatial dislocation of meta-atoms on the focusing phase superposition, both x and y coordinates of $\bar{\varphi}_{\text{cross}}$ are corrected by half a period. In sample 1, the focal length in Eqs. (8)–(10) is $f = 7$ mm, and the wavelength is $\lambda = 273$ μm. The simulated and measured results for electric field intensity of sample 1 at the focal plane are shown in Fig. 3(c), where all the values are normalized, and the design frequency is 1.1 THz. They are obtained from a full-wave simulation of the transmitted electric field under the illumination of x- and y-polarized waves, and the specific simulation settings are explained in Appendix A. In order to clearly show the polarization state of the transmitted beam, we give the simulation results of two orthogonal polarization components, including a 2D intensity and a 1D curve of the central section. As can be seen in the figure, the RCP and the b-polarized components are the main parts, while the orthogonal polarization components are very weak, which is consistent with our design. The corresponding experimental results of sample 1 are shown in the second line of Fig. 3(c), where the actual frequency is 1.08 THz at the plane of $z = 6.8$ mm. They are basically in agreement with the simulation results of the first line. The phase distributions which indicate the mode order of the generated vortex beam are shown in Appendix C (Fig. 8). For specific measurement steps, see Appendix A. In addition, we also consider the working bandwidth of the metasurface, taking the incidence of x-polarized wave as an example. Figure 3(d) shows the electric field intensity distributions in the xoz-plane of several frequencies near 1.1 THz, in which the focusing efficiencies are relatively high. Due to the high refractive index of silicon in the terahertz band ($n = 3.45$ around 1 THz), the reflection is up to 30% at the air/silicon interface under normal incidence [34]. Here we only focus on the transmitted part. Figure 3(e) shows the polarization conversion efficiency in the range of 0.7–1.4 THz, which is obtained at the focal plane ($z = 7$ mm) by

$$\eta = \frac{|E_{\text{RCP}}|^2}{|E_{\text{RCP}}|^2 + |E_{\text{LCP}}|^2}. \tag{11}$$

It can be seen that the conversion efficiency at the design frequency of 1.1 THz is up to 89.2%, and it is greater than 60% in the entire survey frequency band. The simulated results show that the efficiency is higher than 80% in the range of 0.8–1.3 THz, with a peak value of 93.8% at 1.1 THz. The measured values are slightly smaller than the simulated ones; after all, there are some noise signals in the edge area of the focal plane in the measurement results.

In fact, we can obtain more channels in one metasurface via area division of the sample, which means designing different phase distributions in different areas [30]. For simplicity, we only consider the condition of dividing the effective area into two sub-arrays. When the x- or y-polarized wave is incident, the two areas produce different circularly polarized beams. To this end, we design and process the sample 2 shown in Fig. 4(a), where the phase functions of the left- and right-half regions are

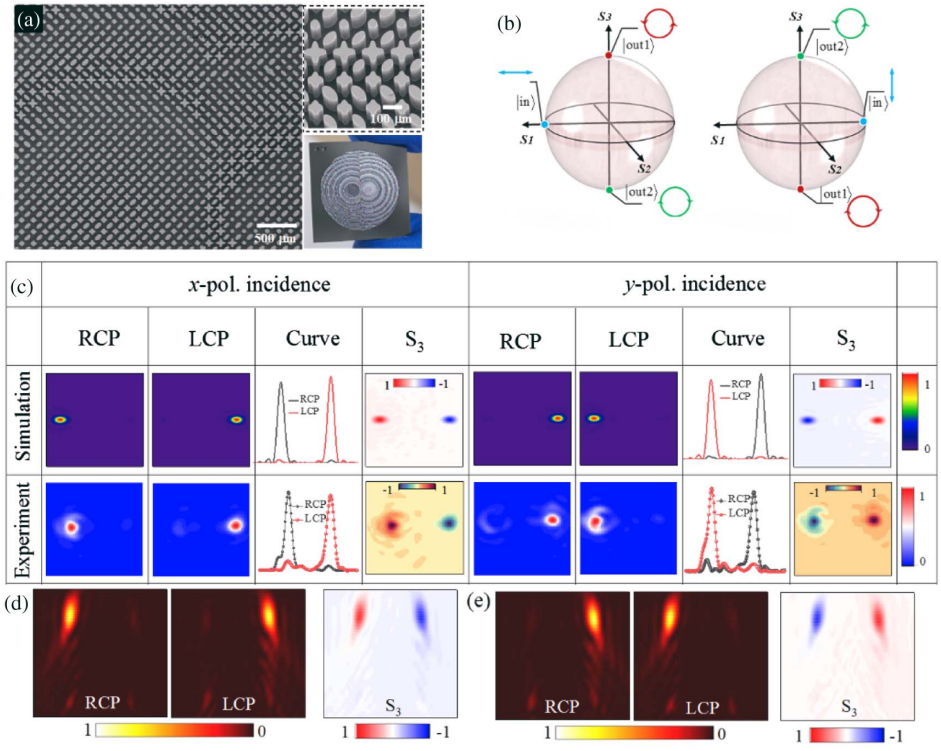

Fig. 4. Simulated and experimental results of sample 2 for the generation of focused vortex beam with polarization conversion. (a) SEM image and optical photo of sample 2. (b) Demonstration of the dual-channel polarization conversion on the Poincaré sphere. (c) Electric field intensity of the transmitted wave when the x- or y-polarized beam is incident. (d), (e) Electric field intensity in the longitudinal section (xoz-plane) for different polarization components, and values of S_3 component of the Stokes parameters.

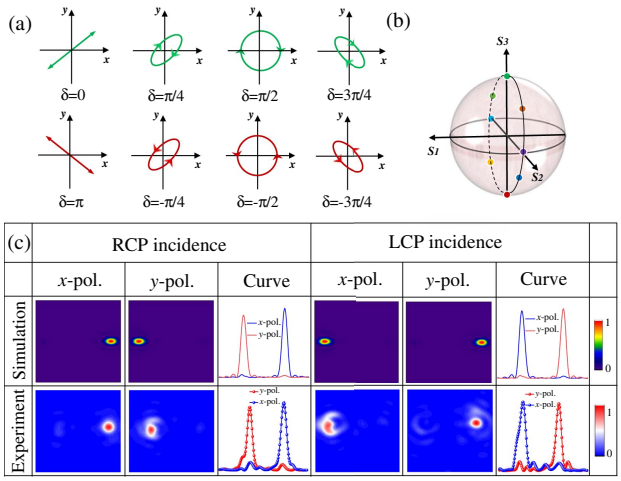

Fig. 5. General discussions on the available polarization states. (a), (b) The possible polarization realization of the transmitted wave when the linearly polarized wave is incident. (c) Transmitted electric field intensities under circularly polarized wave illumination.

shown in Appendix B (Fig. 7). The focal length of sample 2 is $f = 7$ mm, and the working wavelength is $\lambda = 273$ μm. The Poincaré sphere in Fig. 4(b) shows the polarization conversion function of sample 2. At this time, one input linear polarization state can generate two output circular polarization states at different positions. Figure 4(c) shows the polarization components of the transmitted electric field when the *x*- or *y*-polarized wave is incident. In addition to the electric field intensity and section curve similar to Fig. 3(c), here we also use the S_3 component (normalized) of Stokes parameters to intuitively show the circular polarization distribution of the transmitted wave. It can be seen that both left- and right-handed circular polarizations have been obtained efficiently, and the simulation results are in agreement with the experimental data. In addition, we show the electric field intensity and S_3 parameter distributions of the metasurface in the longitudinal section (*xoz*-plane) in Fig. 4(d). It can be found that the division of the regions does not significantly affect the focusing efficiency of the metasurface.

Generally, in the case where linearly polarized waves are incident, all the polarization states we get are derived from the superposition of orthogonal linearly polarized components transmitted by the two types of meta-atoms. With different phase shifts, various states such as linear, elliptical, or circular polarization can be obtained. In particular, when the *x*- or *y*-polarized wave is incident, both of the polarization components appear in the transmitted beam. Assuming that the phase difference between the *x* and *y* polarization components in the transmission is $\delta = \delta_x - \delta_y$, Fig. 5(a) shows the generated polarization states when δ takes different values. The corresponding positions on the Poincaré sphere are shown in Fig. 5(b). It should be noted that when only the *x*- or *y*-polarized wave is incident, we will never get a purely *x*- or *y*-polarized transmitted wave. However, as shown in Fig. 5(c), when the RCP or LCP wave is incident in sample 2, we can get *x*- or *y*-polarized beams. In this way, we have achieved the coverage of various typical polarizations of the transmitted wave.

3. CONCLUSION

In summary, we propose a new method for terahertz beam shaping with multi-channel polarization conversion based on all-silicon metasurfaces. We alternately arrange two kinds of meta-atoms in a single metasurface, eigen-polarizations of which are *x*, *y*, or ±45° polarizations, respectively. Therefore, when *x*- or *y*-polarized waves are incident, they will respectively generate co- or cross-polarized transmitted waves while achieving beam shaping. In this way, a new polarization state in transmission can be obtained after far-field interference, and there are two independent channels available. In addition, a single metasurface can be divided into two or even more subarrays to achieve more channels for polarization conversion or beam shaping. To this end, we designed and processed two samples to demonstrate the above functions. The simulated and experimental results of the first sample verify the dual-channel polarization conversion with linearly polarized incidence. The second one shows the multi-channel polarization conversion controlled by polarization incidence and region division. We use electric field intensities, Stokes parameters, and Poincaré spheres to show the working performance of the metasurface, which confirm our proposed scheme. The experimental results of the electric field are in agreement with the simulations. This design method is not only easier to implement and can provide independent polarization conversion channels, but can also be extended from a linear polarization base to a circular polarization base. The proposed metasurfaces are expected to be applied for polarization multiplexing imaging, holography, and detection of polarization state of terahertz wave.

APPENDIX A: EXPERIMENTAL SECTION

Numerical simulations: We simulate the meta-atoms and whole samples using the commercial software CST MICROWAVE STUDIO (2019, time domain solver). We first calculate the transmission amplitudes and phases of the units with different geometric dimensions. At this time, both *x* and *y* directions are set as periodic boundaries, and the open boundary is set along the *z* direction, while a plane wave is used as the excitation source. Based on the parameter libraries, we use a MATLAB code to drive the CST MICROWAVE STUDIO to draw the whole structure of the sample. Then the *x*, *y*, and *z* directions are set as open boundary conditions, and the calculation space in the *z* direction is larger than the designed focal length. Finally, another MATLAB code is used to process the simulation results when needed.

Experimental setup: We measure the electric field intensity and phase distributions of the focused terahertz beam (Figs. 3–5) using the two-dimensional electro-optical sampling imaging system (Appendix E, Fig. 7). The system contains a pump module and a probe module, supported by a femtosecond laser amplifier system (pulse width is 50 fs, working wavelength is 800 nm, repetition frequency is 1 kHz). During the measurement, we put the sample in the proper position to make the incident wave be *x*- or *y*-polarized, and we measure the two orthogonal linear polarization components in the transmitted beam. Then the sample is rotated 90° around the transmission direction to measure the two polarization components again, and finally the circular polarization

components in the transmitted wave can be obtained through polarization calculation.

Sample fabrication: Ultraviolet lithography and ICP etching are used to process the samples. We use standard photolithography to form a 6.8 μm thick patterned positive photoresist (AZ4620) as a mask on a 500 μm thick silicon wafer with a diameter of 4 inch (1 inch = 2.54 cm). Then we use (ICP) etching technology (STS MULTIPLEX ASE-HRM ICP ETCHER, United Kingdom) to etch the sample, and finally the remaining photoresist is washed away to get the final sample. The etching depth is about 200 μm, and the remaining 300 μm thick silicon layer is used as the substrate.

APPENDIX B: GEOMETRIC SIZE SELECTION OF THE META-ATOMS

In order to obtain the parameter library of the two types of meta-atoms, we simulated the amplitudes and phases of the transmitted wave with their lateral dimensions as variables (the height of the silicon pillar is 200 μm, and thickness of the substrate is 300 μm). The results are shown in Fig. 6, where Figs. 6(a)–6(d) are the simulation results of type (i), and Figs. 6(e), 6(f) are the results of type (ii). The values of w_1 and w_2 are increased from 40 to 130 μm, while w_3 and w_4 are from 40 to 70 μm, and the increase step length of all the variables is 2 μm. Based on these results, we get the chosen values in Figs. 2(b)–2(f) in the paper.

APPENDIX C: PHASE DISTRIBUTION FUNCTIONS OF SAMPLE 2

As mentioned in the paper, the effective area of sample 2 is divided into two sub-arrays, in which the phase distribution functions of the two types of meta-atoms in the left half ($x < 0$) and the right half ($x > 0$) are as follows:

$$\bar{\varphi}_{xx} = -\left(\frac{2\pi}{\lambda}\sqrt{(x-1200)^2+y^2+f^2}-f\right)-\frac{\pi}{2}, \quad x<0, \tag{C1}$$

$$\bar{\varphi}_{yy} = -\left(\frac{2\pi}{\lambda}\sqrt{(x-1200)^2+y^2+f^2}-f\right)-\frac{\pi}{2}, \quad x<0, \tag{C2}$$

$$\bar{\varphi}_{\text{cross}} = -\left(\frac{2\pi}{\lambda}\sqrt{\left(x+\frac{p}{2}-1200\right)^2+\left(y-\frac{p}{2}\right)^2+f^2}-f\right), \quad x<0, \tag{C3}$$

$$\bar{\varphi}_{xx} = -\left(\frac{2\pi}{\lambda}\sqrt{(x+1200)^2+y^2+f^2}-f\right)+\frac{\pi}{2}, \quad x>0, \tag{C4}$$

$$\bar{\varphi}_{yy} = -\left(\frac{2\pi}{\lambda}\sqrt{(x+1200)^2+y^2+f^2}-f\right)+\frac{\pi}{2}, \quad x>0, \tag{C5}$$

$$\bar{\varphi}_{\text{cross}} = -\left(\frac{2\pi}{\lambda}\sqrt{\left(x+\frac{p}{2}+1200\right)^2+\left(y-\frac{p}{2}\right)^2+f^2}-f\right), \quad x>0. \tag{C6}$$

As with sample 1, we have also introduced a half-period correction in the focusing phase function of the second type of meta-atoms to eliminate the degradation of polarization conversion efficiency that may be caused by spatial dislocation.

In order to show the near-field phase distributions of the metasurface more intuitively, we draw the phase profile of the two samples according to Eqs. (8)–(10) and Eqs. (C1)–(C6) above, as shown in Fig. 7. Sample 1 is a single focused vortex

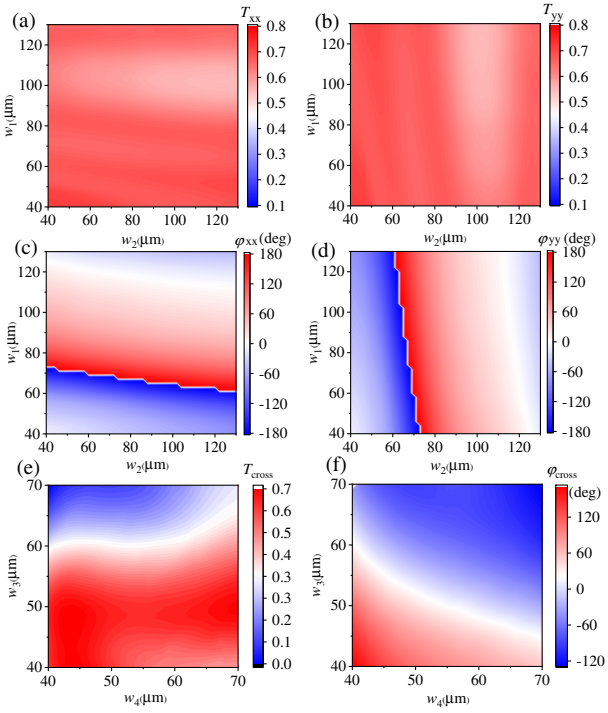

Fig. 6. Transmission amplitudes and phases of the meta-atoms with different geometric sizes.

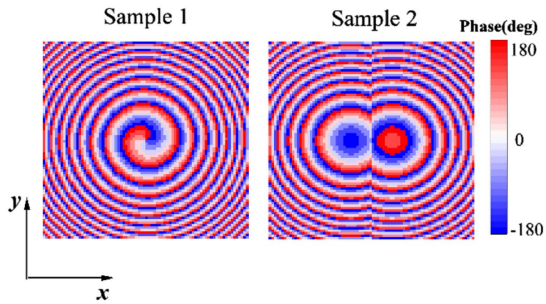

Fig. 7. Near-field phase distributions of the two samples.

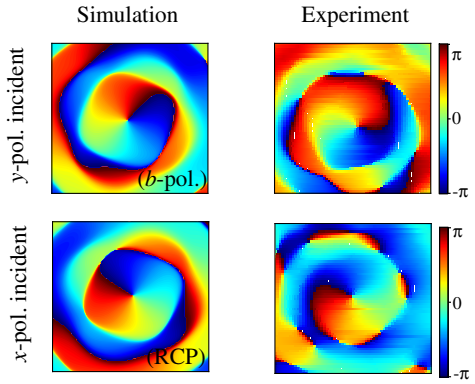

Fig. 8. Phase distributions in the focal plane of the generated vortex beam from sample 1.

beam, while sample 2 is divided into two regions, both of which are focused phase profiles.

The phase distributions in the focal plane which indicate the mode order of the generated vortex beam from sample 1 are shown in Fig. 8. When the y-polarized (x-polarized) wave is incident, we only show the transmitted b-polarized (RCP) component. Obviously, the simulated and measured results show that the topological charge of the generated vortex beam is $l = 1$, which also meets the description of Eqs. (8)–(10).

APPENDIX D: TERAHERTZ IMAGING SYSTEM

We measure the electric field intensity and phase distributions of the focused terahertz beam (Figs. 3–5 in the paper) using the two-dimensional electro-optical sampling imaging system in Fig. 9. The system includes a pump module and a probe module, supported by a femtosecond laser amplifier system (pulse width is 50 fs, working wavelength is 800 nm, repetition frequency is 1 kHz). In the pump module, a pump beam from the femtosecond laser is irradiated on the electro-optic crystal ZnTe to excite terahertz pulses, and then the terahertz beam is collimated by an off-axis parabolic mirror and irradiated on the sample. While in the probe module, the other beam is incident to another ZnTe crystal to probe the terahertz electric field. The optical imaging module is composed of two lenses, including a Wollaston prism (polarizing beam splitter, PBS), a quarter-wave plate, and a CCD camera. To measure the cross-polarized terahertz wave, the polarization state of the probe beam can be changed by using the half-wave plate and the polarizer. In addition, we rotate the sample to be equivalent to the polarization change of the incident terahertz wave.

APPENDIX E: MEASUREMENT OF THE POLARIZATION CONVERSION FOR TERAHERTZ WAVE

The imaging system we use can only generate a linearly polarized terahertz beam in the pump module, while the probe module can measure the linearly co- and cross-polarized components. Therefore, the transmitted circularly polarized wave can be obtained if we superimpose the measured x and y polarization components for sample 1, which is also applicable to

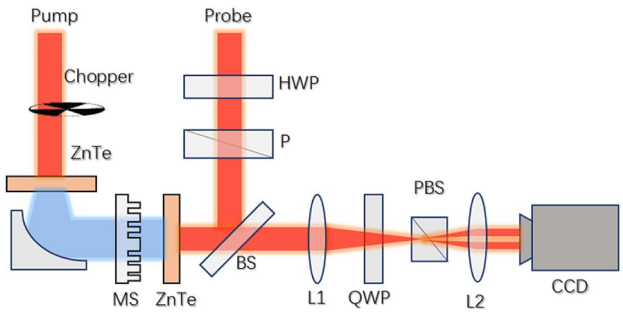

Fig. 9. THz imaging system based on two-dimensional electro-optical sampling.

the case of sample 2 when linearly polarized waves are incident:

$$E^{\sigma} = \frac{E_x - i\sigma E_y}{\sqrt{2}}, \tag{E1}$$

where $\sigma = \pm 1$ means the left- or right-handed circularly polarized waves, respectively.

For the condition where the circularly polarized wave is incident in sample 2, after measuring four linear polarization components, circularly polarized components in the transmitted beam can be obtained according to the following formula, and then the final polarization state can be judged:

$$\begin{pmatrix} E_{++} & E_{+-} \\ E_{-+} & E_{--} \end{pmatrix} = \frac{1}{2}\begin{pmatrix} E_{xx} + E_{yy} + i(E_{xy} - E_{yx}) & E_{xx} - E_{yy} - i(E_{xy} + E_{yx}) \\ E_{xx} - E_{yy} + i(E_{xy} + E_{yx}) & E_{xx} + E_{yy} - i(E_{xy} - E_{yx}) \end{pmatrix}, \tag{E2}$$

where $E_{i,j}$ $(i, j = +, -)$ represents the four circular polarization components.

Funding. National Natural Science Foundation of China (61675147, 61735010, 91838301); National Key Research and Development Program of China (2017YFA0700202); Basic Research Program of Shenzhen (JCYJ20170412154447469).

Disclosures. The authors declare no conflicts of interest.

REFERENCES

1. M. Onoda, S. Murakami, and N. Nagaosa, "Hall effect of light," Phys. Rev. Lett. **93**, 083901 (2004).
2. O. Hosten and P. Kwiat, "Observation of the spin Hall effect of light via weak measurements," Science **319**, 787–790 (2008).
3. W. Groner, J. W. Winkelman, A. G. Harris, C. Ince, G. J. Bouma, K. Messmer, and R. G. Nadeau, "Orthogonal polarization spectral imaging: a new method for study of the microcirculation," Nat. Med. **5**, 1209–1212 (1999).
4. T. Stav, A. Faerman, E. Maguid, D. Oren, V. Kleiner, E. Hasman, and M. Segev, "Quantum entanglement of the spin and orbital angular momentum of photons using metamaterials," Science **361**, 1101–1104 (2018).

5. R. C. Devlin, A. Ambrosio, N. A. Rubin, J. P. B. Mueller, and F. Capasso, "Arbitrary spin-to-orbital angular momentum conversion of light," Science **358**, 896–901 (2017).
6. D. Goldstein, *Polarized Light*, 3rd ed. (CRC Press, 2010).
7. N. Yu and F. Capasso, "Flat optics with designer metasurfaces," Nat. Mater. **13**, 139–150 (2014).
8. Q. Zhao, J. Zhou, F. Zhang, and D. Lippens, "Mie resonance-based dielectric metamaterials," Mater. Today **12**, 60–69 (2009).
9. S. Sun, Q. He, S. Xiao, Q. Xu, X. Li, and L. Zhou, "Gradient-index meta-surfaces as a bridge linking propagating waves and surface waves," Nat. Mater. **11**, 426–431 (2012).
10. Y. Yu, A. Y. Zhu, R. Paniagua-Dom´ınguez, , Y. Fu, B. Luk'yanchuk, and A. I. Kuznetsov, "High-transmission dielectric metasurface with 2π phase control at visible wavelengths," Laser Photonics Rev. **9**, 412–418 (2015).
11. F. Zangeneh-Nejad, D. L. Sounas, A. Alù, and R. Fleury, "Analogue computing with metamaterials," Nat. Rev. Mater. **6**, 207–225 (2021).
12. Y. Zhou, H. Zheng, I. I. Kravchenko, and J. Valentine, "Flat optics for image differentiation," Nat. Photonics **14**, 1–2 (2020).
13. G. Li, S. Zhang, and T. Zentgraf, "Nonlinear photonic metasurfaces," Nat. Rev. Mater. **2**, 17010 (2017).
14. S. Chen, G. Li, K. W. Cheah, T. Zentgraf, and S. Zhang, "Controlling the phase of optical nonlinearity with plasmonic metasurfaces," Nanophotonics **7**, 1013–1024 (2018).
15. Q. Wang, E. Plum, Q. Yang, X. Zhang, Q. Xu, Y. Xu, J. Han, and W. Zhang, "Reflective chiral meta-holography: multiplexing holograms for circularly polarized waves," Light Sci. Appl. **7**, 25 (2018).
16. Z. Zhang, M. Kang, X. Zhang, X. Feng, Y. Xu, X. Chen, H. Zhang, Q. Xu, Z. Tian, W. Zhang, A. Krasnok, J. Han, and A. Alù, "Coherent perfect diffraction in metagratings," Adv. Mater. **32**, 2002341 (2020).
17. Z. Wang, S. Li, X. Zhang, X. Feng, Q. Wang, J. Han, Q. He, W. Zhang, S. Sun, and L. Zhou, "Excite spoof surface plasmons with tailored wavefronts using high-efficiency terahertz metasurfaces," Adv. Sci. **7**, 2000982 (2020).
18. J. J. Baumberg, J. Aizpurua, M. H. Mikkelsen, and D. R. Smith, "Extreme nanophotonics from ultrathin metallic gaps," Nat. Mater. **18**, 668–678 (2019).
19. D. Neshev and I. Aharonovich, "Optical metasurfaces: new generation building blocks for multi-functional optics," Light Sci. Appl. **7**, 58 (2018).
20. D. Wang, F. Liu, T. Liu, S. Sun, Q. He, and L. Zhou, "Efficient generation of complex vectorial optical fields with metasurfaces," Light Sci. Appl. **10**, 67 (2021).
21. Z. Shi, A. Y. Zhu, Z. Li, Y. Huang, W. Chen, C. W. Qiu, and F. Capasso, "Continuous angle-tunable birefringence with freeform metasurfaces for arbitrary polarization conversion," Sci. Adv. **6**, eaba3367 (2020).
22. S. Wang, Z. Deng, Y. Wang, Q. Zhou, X. Wang, Y. Cao, B. Guan, S. Xiao, and X. Li, "Arbitrary polarization conversion dichroism metasurfaces for all-in-one full Poincaré sphere polarizers," Light Sci. Appl. **10**, 24 (2021).
23. Q. Fan, M. Liu, C. Zhang, W. Zhu, Y. Wang, P. Lin, F. Yan, L. Chen, H. J. Lezec, Y. Lu, A. Agrawal, and T. Xu, "Independent amplitude control of arbitrary orthogonal states of polarization via dielectric metasurfaces," Phys. Rev. Lett. **125**, 267402 (2020).
24. S. Gao, C. Park, C. Zhou, S. Lee, and D. Choi, "Twofold polarization-selective all-dielectric trifoci metalens for linearly polarized visible light," Adv. Opt. Mater. **7**, 1900883 (2019).
25. J. Li, L. Zhang, M. Zhang, H. Su, I. L. Li, S. Ruan, and H. Liang, "Wearable conformal metasurfaces for polarization division multiplexing," Adv. Opt. Mater. **8**, 2000068 (2020).
26. Y. Yuan, K. Zhang, B. Ratni, Q. Song, X. Ding, Q. Wu, S. N. Burokur, and P. Genevet, "Independent phase modulation for quadruplex polarization channels enabled by chirality-assisted geometric-phase metasurfaces," Nat. Commun. **11**, 4186 (2020).
27. Y. Yuan, S. Sun, Y. Chen, K. Zhang, X. Ding, B. Ratni, Q. Wu, S. N. Burokur, and C. W. Qiu, "A fully phase-modulated metasurface as an energy-controllable circular polarization router," Adv. Sci. **7**, 2001437 (2020).
28. A. Pors, M. G. Nielsen, and S. I. Bozhevolnyi, "Plasmonic metagratings for simultaneous determination of Stokes parameters," Optica **2**, 716–723 (2015).
29. Y. Gao, X. Xiong, Z. Wang, F. Chen, R. Peng, and M. Wang, "Simultaneous generation of arbitrary assembly of polarization states with geometrical-scaling-induced phase modulation," Phys. Rev. X **10**, 031035 (2020).
30. F. Ding, B. Chang, Q. Wei, L. Huang, X. Guan, and S. I. Bozhevolnyi, "Versatile polarization generation and manipulation using dielectric metasurfaces," Laser Photonics Rev. **14**, 2000116 (2020).
31. J. P. B. Mueller, N. A. Rubin, R. C. Devlin, B. Groever, and F. Capasso, "Metasurface polarization optics: independent phase control of arbitrary orthogonal states of polarization," Phys. Rev. Lett. **118**, 113901 (2017).
32. K. Zhang, Y. Yuan, X. Ding, B. Ratni, S. N. Burokur, and Q. Wu, "High efficiency metalenses with switchable functionalities in microwave region," ACS Appl. Mater. Interfaces **11**, 28423–28430 (2019).
33. M. Liu, W. Zhu, P. Huo, L. Feng, M. Song, C. Zhang, L. Chen, H. J. Lezec, Y. Lu, A. Agrawal, and T. Xu, "Multifunctional metasurfaces enabled by simultaneous and independent control of phase and amplitude for orthogonal polarization states," Light Sci. Appl. **10**, 107 (2021).
34. H. Zhang, X. Zhang, Q. Xu, C. Tian, Q. Wang, Y. Xu, Y. Li, J. Gu, Z. Tian, C. Ouyang, X. Zhang, C. Hu, J. Han, and W. Zhang, "High-efficiency dielectric metasurfaces for polarization-dependent terahertz wavefront manipulation," Adv. Opt. Mater. **6**, 1700773 (2018).